

Imaging scanning tunneling microscope-induced electroluminescence in plasmonic corrals

Shunji Egusa

Department of Physics, James Franck Institute, and Materials Research Science and Engineering Center,
The University of Chicago, Chicago, Illinois 60637

Yish-Hann Liao and Norbert F. Scherer^{a)}

Department of Chemistry, James Franck Institute, and Materials Research Science and Engineering Center,
The University of Chicago, Chicago, Illinois 60637

(Received 14 October 2003; accepted 19 December 2003)

An approach to image localized and propagating surface plasmon (SP) modes is introduced. It is shown that scanning tunneling microscope (STM)-electroluminescence, the radiative decay of SPs induced by inelastically tunneling electrons, observed in Fourier space yields distinct features that reflect the degree of delocalization and spatial distribution of SP modes. The propagating SP is isolated from the localized mode by way of this Fourier space imaging approach. Furthermore, a cylindrically symmetric spatial interference pattern is obtained when the STM-induced plasmon is created within a circular “corral” boundary condition. © 2004 American Institute of Physics.
[DOI: 10.1063/1.1649799]

The prospect of creating photonic devices based on surface plasmon propagation is attracting increasing attention.^{1–5} The motivation has been to create miniaturized optics that would enable higher bandwidth optical computing, all-optical interconnects for telecommunications, or even “nano-lasers.” Whereas the miniaturization of conventional dielectric optics is fundamentally restricted by the diffraction limit, surface plasmons (SPs) are not similarly limited.⁶ SPs are electromagnetic modes, or charge density waves, that exist at metal–dielectric interfaces with their field amplitudes decaying exponentially in the neighboring media. They propagate in extended one-dimensional and two-dimensional structures⁷ and can exist within and couple between single nano-scale metal particles,⁸ enabling manipulation of “light” at the nano-scale. In conjunction with recent developments in nano-fabrication, transducing light into SP modes could realize nano-scale optical devices^{6,9} that may allow integration with nano-scale electronics.

Device development requires understanding the dynamics of SPs in such nano-structures, including mapping the spatial distribution of SP modes. Near-field scanning optical microscopies have been utilized to study propagating SPs scattering from simple objects on films. However, distinguishing between plasmon modes and optical modes^{10,11} may not be trivial.

The tunneling current from a biased scanning tunneling microscope (STM) tip can excite SP modes in metal films¹² and nano-particles¹³ by inelastic electron tunneling. The photon yield per electron resulting from the radiative decay of these modes is highly dependent on the size of the nanostructures,¹³ in excellent agreement with theory.¹⁴ Elucidation of spatial emission patterns would be an important extension bringing greater insight to plasmon propagation, confinement, and energetics.

This letter introduces a method to excite, distinguish,

and map localized and propagating SP modes. Tunneling electrons from a STM tip are used as a nano-scale non-optical excitation source of SP modes in unstructured and submicron structured Au film samples. Photon emission patterns originating from the radiative decay of these SP modes are studied herein by Fourier space imaging. Two types of SP modes with distinct length scales are observed: a *tip-localized mode* resulting from a resonance at the STM tip apex scale, which is transduced into a *propagating mode* on flat Au surfaces.^{15,16} Both modes can decay radiatively, mediated by surface roughness, and hence are observable with far-field optics.

The experimental setup is shown in Fig. 1.¹³ The ambient, room temperature STM (Bioscope, Digital Instruments) was operated in constant current mode with tunneling current $I = 10$ nA; the chemically etched Pt/Ir tip was negatively bi-

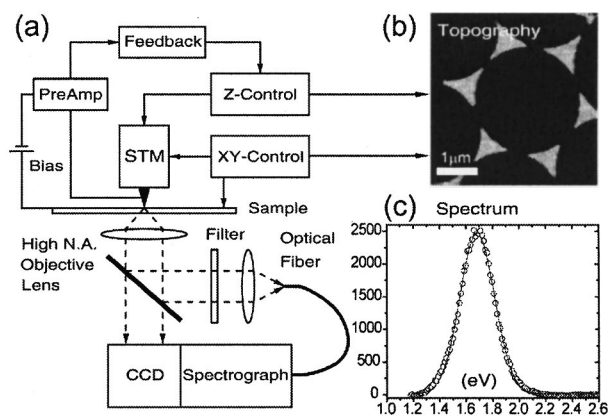


FIG. 1. Experimental scheme. The STM scanner is mounted on the stage of an inverted microscope such that the STM tip is aligned with the optical axis of a high numerical aperture objective lens. The apparatus is housed in an acoustic isolation enclosure and is mounted on an active anti-vibration system and a floating vibration isolation table. (b) STM topography of a circular corral formed by six cusped triangular Au islands, on a 35 nm Au film. (c) Spectrum of photon emission from the SP in the corral, obtained with a bias voltage of 2.3 V.

^{a)}Electronic mail: nfschere@uchicago.edu

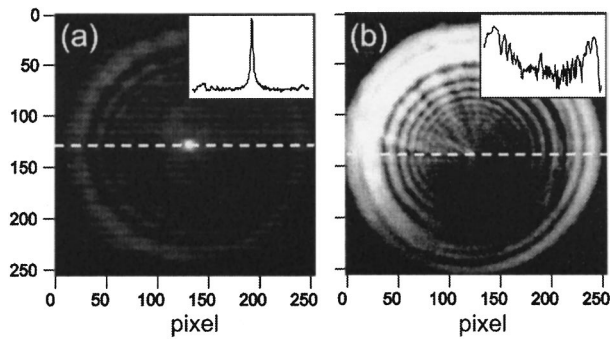


FIG. 2. Emission patterns (256×256 pixels, $26 \times 26 \mu\text{m}^2$ per pixel, and log intensity scale) from (a) Au film and (b) Au plasmonic corral. The cross section through the center (dashed line) is shown as an inset. In (b), the STM tip is positioned over the exact center of the circular corral. The applied bias voltage is 2.3 V and the acquisition time is 300 s.

used with respect to the sample. A $60\times/\text{NA}=1.45$ oil immersion objective lens (Olympus, Apochromat) located under the sample was aligned with the STM tip and collected the STM-induced photon emission with the range of angles limited by $\theta_{\text{NA}}=75^\circ$ with respect to the optical axis. The emission patterns¹⁷ were obtained by collimating the photon emission and projecting it onto a liquid nitrogen cooled CCD array detector (JY Horiba). For spectral measurements, the photon emission was injected into an optical fiber with an achromat lens and coupled to a holographic grating spectrograph (Kaiser Optical Systems) integrated with the same CCD detector. The wavelength scale of the spectrograph was calibrated with a Hg/Ar lamp from 1.15 to 2.55 eV, and the spectral response was corrected with a tungsten lamp.

The samples were made by electron beam evaporation of Au in high vacuum (1×10^{-6} Torr). The typical surface roughness, determined by atomic force microscopy, was 1 nm rms. Hexagonal lattices of triangularly shaped Au islands ($\sim 1 \mu\text{m}$ across and 35 nm in height) were prepared on Au films (35 nm in thickness) using a self-assembled close-packed monolayer of latex spheres ($2.4 \pm 0.1 \mu\text{m}$ in diameter, Interfacial Dynamics Corp.) as a mask.¹⁸ The circular “corral” structures thus formed, each defined by six cusped-triangular Au islands surrounding the Au film region, create a circular boundary for propagating SP modes excited in the underlying Au film. Figure 1(b) is the STM topography of the sample taken with the same operational parameters as the photon emission experiment. The photon emission spectrum [see Fig. 1(c)] from the sample of Fig. 1(b) exhibits a peak at 1.68 eV ($\lambda = 738 \text{ nm}$). This information is used to confirm the real space scale of the Fourier transformed images.

Figure 2 shows the emission patterns recorded by the CCD detector for the (a) Au film and (b) Au corral samples. The emission pattern in Fig. 2(b) is measured with the STM tip positioned over the center of the circular corral. The emission patterns from both samples exhibit a similar broad annular feature at large NA. The striking difference occurs inside the annular feature; a distinct sharp peak is observed from the Au film sample at $\text{NA}=0$ (i.e., on-axis), whereas more complicated features are observed with the Au corral sample. Information about the spatial structure of the radiating SP modes can be obtained by Fourier transforming these reciprocal space data.

An image formed by a lens is a Fourier transform of the

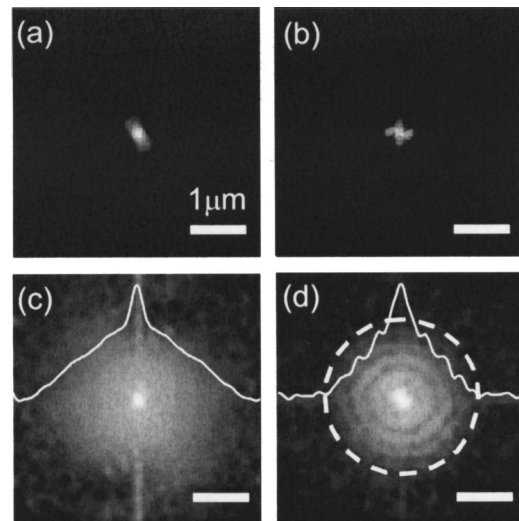


FIG. 3. Fourier transformed images (log intensity scale) of the selected features in the emission patterns shown in Fig. 2: (a) Au film/annulus, (b) Au plasmonic corral/annulus, (c) Au film/inside annulus, and (d) Au plasmonic corral/inside annulus. The dashed circle in (d) represents the corral boundary. The cross section through the center is shown as the superimposed curve in (c) and (d).

source.¹⁹ Consider a light ray with a wave vector \mathbf{k} originating from a point \mathbf{r} on the source plane. A lens placed at its focal length f away from the source plane collimates the light ray, which is mapped to a point $\boldsymbol{\rho}$ on the image plane. By defining $\mathbf{K} \equiv |\mathbf{k}| \boldsymbol{\rho} / f$, the field $\mathbf{E}_i(\boldsymbol{\rho})$ on the image plane is related to the field $\mathbf{E}_s(\mathbf{r})$ on the source plane via

$$\mathbf{E}_i(\boldsymbol{\rho}) = e^{i\Phi(\boldsymbol{\rho})} \int d^2r \mathbf{E}_s(\mathbf{r}) e^{i\mathbf{K} \cdot \mathbf{r}}. \quad (1)$$

The field $\mathbf{E}_i(\boldsymbol{\rho})$ is the Fourier transform of $\mathbf{E}_s(\mathbf{r})$ up to a phase factor. This relation is accurate for the emission near the optical axis. Emission from an extended region at the source plane would result in a narrow peak at the image plane and vice versa. Therefore, the features seen in Figs. 2(a) and 2(b) near $\text{NA}=0$ reflect the spatial profiles of the delocalized or propagating SP, and the annular feature observed in the two emission patterns is attributed to the radiative decay of the tip-localized SP.

Further interpretation of the data of Fig. 2 is aided by numerically and separately Fourier transforming the annuli and the features near the optical axis. A Hanning filter is used to isolate the ubiquitous annular emission at large NA; the two regions are separated at approximately $\text{NA}=1$. The cylindrical symmetry of the images eliminates the ambiguity of the phase in Fourier transforms, therefore the resultant images, shown in Fig. 3, are the real-space profiles of the SP modes. Figures 3(a) and 3(b) show highly localized and intense emission from the annuli of the CCD images in Figs. 2(a) and 2(b) that reflect the radiative decay of the tip-localized SP mode. Figure 3(c), the Fourier transform of the features inside the annulus of the photon emission pattern from the Au film sample [Fig. 2(a)], exhibits a radially decaying spatial profile. The superimposed line section more clearly shows the exponential decay.⁷ This radiative decay from the propagating SP, with decay length $\sim 2 \mu\text{m}$, is comparable to literature values.²⁰ Figure 3(c) shows a narrow

feature that reflects the finite low-NA emission from a tip-localized point source and tails of the Hanning window.

With the Au corral sample, the spatial profile of the propagating SP is strongly modified due to the boundary condition imposed by the corral. Figure 3(d) clearly shows that the SP is confined by the corral. The propagating SP is reflected at the inner circular edge of the corral constructively interfering with itself, thus forming a standing wave pattern. The confined SP wavelength is $\lambda_{\text{SP}}=703$ nm, deduced from the $2.46 \mu\text{m}$ diameter of the corral as measured from the STM topography. This result is in agreement with the spectral measurement: using the real part of dielectric function of gold $\epsilon'_{\text{Au}}=-19.40$,²¹ the SP wavelength $\lambda_{\text{SP}}=703$ nm obtained from Fig. 3(d) yields a photon emission wavelength of $\lambda=740$ nm, via

$$k_{\text{SP}} = \sqrt{\frac{\epsilon_0 \cdot \epsilon'_{\text{Au}}}{\epsilon_0 + \epsilon'_{\text{Au}}}} k. \quad (2)$$

The standing wave pattern of Fig. 3(d) is sensitive to the position of the STM tip (SP excitation source) within the corral: the pattern disappears when the tip is slightly displaced from the center of the corral; i.e., the tip is no longer at the anti-node of the corral's (damped) eigenmode.

The STM electroluminescence–Fourier space imaging approach allows excitation of localized and propagating SP modes in nano-structured metal films using a nano-scale source, and also allows separate mapping of different SP modes. Fourier space imaging avoids some complications of considering optical modes or diffraction modifying the excitation. The method as presented will not allow spatial mapping of the SP below the conventional microscopy resolution criteria. However, taking such images in combination with tip raster scanning would allow discrimination of localized and propagating SP modes for photon mapping, and the resolution would be determined by the STM. Namely, collecting only the selected emission features in Fourier space and raster scanning the STM tip would allow mapping the localized and the delocalized SPs with subwavelength spatial resolution. These measurements as well as experiments that excite particle SPs on Au islands, and that determine the influence of the lattice spacing and the topological arrangement of Au islands on the SP standing wave patterns are in progress.

Note added in proof. The ubiquitous annular feature, discussed with respect to Fig. 2, originates from the dipole

emission from the tip-sample junction. The feature inside the annulus is the signal related to surface plasmons.

The authors would like to thank Professor L. Novotny for useful discussions. This work was supported by the University of Chicago MRSEC (NSF-DMR-980895), the W. M. Keck Foundation (991705), and the Consortium for Nanoscience Research, a collaboration with Argonne National Laboratory.

- ¹M. Quinten, A. Leitner, J. R. Krenn, and F. R. Aussenegg, *Opt. Lett.* **23**, 1331 (1998).
- ²M. L. Brongersma, J. W. Hartman, and H. A. Atwater, *Phys. Rev. B* **62**, R16356 (2000).
- ³S. I. Bozhevolnyi, J. Erland, K. Leosson, P. M. W. Skovgaard, and J. M. Hvam, *Phys. Rev. Lett.* **86**, 3008 (2001).
- ⁴J.-C. Weeber, J. R. Krenn, A. Dereux, B. Lamprecht, Y. Lacroute, and J.-P. Goudonnet, *Phys. Rev. B* **64**, 045411 (2001).
- ⁵Y.-H. Liao, S. Egusa, and N. F. Scherer, *Opt. Lett.* **27**, 857 (2002).
- ⁶D. J. Bergman and M. I. Stockman, *Phys. Rev. Lett.* **90**, 027402 (2003).
- ⁷H. Raether, *Surface Plasmons* (Springer, Berlin, 1988).
- ⁸K. Klar, M. Perner, S. Grosse, G. von Plessen, W. Spirkel, and J. Feldmann, *Phys. Rev. Lett.* **80**, 4249 (1998).
- ⁹S. A. Maier, P. G. Kik, and H. A. Atwater, *Appl. Phys. Lett.* **81**, 1714 (2002).
- ¹⁰D. Peyrade, R. Quidant, J. C. Weeber, A. Dereux, G. Leveque, C. Girard, and Y. Chen, *Europhys. Lett.* **56**, 517 (2001).
- ¹¹C. Chicanne, T. David, R. Quidant, J. C. Weeber, Y. Lacroute, E. Bourillot, A. Dereux, G. Colas des Francs, and C. Girard, *Phys. Rev. Lett.* **88**, 097402 (2002).
- ¹²J. H. Coombs, J. K. Gimzewski, J. K. Reihl, J. K. Sass, and R. R. Schlitter, *J. Microsc.* **152**, 325 (1988).
- ¹³Y.-H. Liao and N. F. Scherer, *Appl. Phys. Lett.* **74**, 3966 (1999).
- ¹⁴B. N. J. Persson and A. Baratoff, *Phys. Rev. Lett.* **68**, 3224 (1992).
- ¹⁵T. Kume, N. Nakagawa, S. Hayashi, and K. Yamamoto, *Solid State Commun.* **93**, 171 (1995).
- ¹⁶Y. Uehara, Y. Kimura, S. Ushioda, and K. Takeuchi, *Jpn. J. Appl. Phys., Part 1* **31**, 2465 (1992).
- ¹⁷It was verified that these patterns were free of optical artifacts by inserting an achromat lens in the collimated beam path and obtaining an image identical to a known object (i.e., sample) when the CCD is placed at the image plane of the lens. Similarly, the object could be faithfully reproduced by Fourier transformation when the CCD was at the Fourier plane, with or without the lens.
- ¹⁸T. R. Jensen, M. D. Malinsky, C. L. Haynes, and R. P. Van Duyne, *J. Phys. Chem. B* **104**, 10549 (2000).
- ¹⁹J. W. Goodman, *Introduction to Fourier Optics*, 2nd ed. (McGraw-Hill, New York, 1996).
- ²⁰P. Dawson, B. A. F. Puygranier, and J.-P. Goudonnet, *Phys. Rev. B* **63**, 205410 (2001).
- ²¹E. D. Palik, *Handbook of Optical Constants of Solids* (Academic, San Diego, 1998).